Model-Based Pitch Angle Compensation for Center of Gravity Variation in Underactuated System with an Arm

1st Hirotaka Kanazawa
Graduate School of Integrated Design Engineering, Keio University
Yokohama, Japan
kanazawa@sum.sd.keio.ac.jp

2nd Kosuke Ishizaki
Toyota Industries Corporation
Obu-shi, Japan
kosuke.ishizaki@mail.toyota-shokki.co.jp

3rd Yasuhiro Miyata
Toyota Industries Corporation
Obu-shi, Japan
yasuhiro.miyata@mail.toyota-shokki.co.jp

4th Masamichi Nawa
Toyota Industries Corporation
Obu-shi, Japan
masamichi.nawa@mail.toyota-shokki.co.jp

5th Norihiko Kato
Toyota Industries Corporation
Obu-shi, Japan
norihiko.kato@mail.toyota-shokki.co.jp

6th Toshiyuki Murakami
Department of System Design Engineering, Keio University
Yokohama, Japan
mura@sd.keio.ac.jp

2023 IEEE 32nd International Symposium on Industrial Electronics (ISIE) | 979-8-3503-9971-4/23/$31.00 ©2023 IEEE | DOI: 10.1109/ISIE51358.2023.10228009

***Abstract*—Two-wheeled robots are expected to be used at sites where humans work together. The subject of this paper is a two-wheeled robot with an arm, which can take out loads from shelves in the same manner as a human. When the center of gravity (CoG) of the two-wheeled robot shifts back and forth due to placing a load on the arm, the wheel position control performance deteriorates. A possible method to compensate for the shift in the CoG is to use repulsive compliance control (RCC). However, RCC has the disadvantages that the parameters must be adjusted experimentally and the CoG compensation is slow because the pitch angle is determined dynamically. To address these disadvantages, this paper proposes a method that uses model-based CoG compensation and position control for pitch angle. The model-based controller design simplifies parameter setting and achieves fast CoG compensation by statically determining the desired pitch angle. The validity of the proposed method is confirmed through experiments. The obtained results show that the performance of wheel position control is improved when the load is placed on the arm.**

***Index Terms*—Two-wheeled robot, Center of gravity compensation, Model-based control**

I. Introduction

In recent years, labor shortages have become a serious issue due to the declining birthrate and aging population all over the world. Automation by robots is expected to compensate for labor shortages in factories and warehouses. Factories and warehouses are designed for people with the characteristics of a small footprint and high center of gravity (CoG). Therefore, robots must also have a small footprint and high CoG to work like a person in these environments. Two-wheeled robots (TWRs) can maintain balance even with a high CoG and a small footprint structure.

The TWRs are underactuated systems that have three degrees of freedom: posture and position (x and y) of the vehicle body with two actuators on the left and right wheels. Although TWRs are statically unstable, the tilt of the vehicle body can be stabilized by controlling the wheel motors. Because of these advantages, research on TWR has been widely conducted [1]. Pathak et al. analyzed the dynamics of a wheeled inverted pendulum and achieved velocity and position tracking to target values while controlling the pitch angle within a specified range by applying partially linearized feedback [2]. Nakamura et al. introduced two types of disturbance observers (DOBs) to a TWR and achieved posture stabilization using a method based on the Lyapunov stability theorem [3]. One DOB compensates for disturbances that the wheels receive from the ground, and the other DOB, called a pitch angle disturbance observer (PADO), compensates for disturbances applied to the pitch angle. As a result, the control system is robust to disturbances and modeling errors, and a person can ride the TWR. This is called a two-wheeled wheelchair. A synthesized pitch angle disturbance observer (SPADO), which integrates DOB and PADO, has also been developed [4].

Since TWR tilts the body in the direction it wants to move, a typical control strategy is to cascade the pitch angle controller on the inside and the wheel position control on the outside [5]. The performance of wheel position control deteriorates when the body tilts due to placing objects on the TWR or applying disturbances. Therefore, it is necessary to deal with fluctuations in the CoG in the control of a TWR. Acar et al. proposed gravity compensation by repulsive compliance control (RCC) to cope with human CoG shift in a two-wheeled wheelchair [6]. The RCC is a method to suppress the shift of the CoG by dynamically generating a pitch angle command value in the direction that opposes the disturbance applied to the pitch angle according to a set impedance characteristic.

In the research on placing objects on the TWR, Takei et al. proposed a method to compensate for the CoG of the TWR when carrying a load by taking advantage of the fact that the CoG is right above the axle when the TWR is stationary [7].

To compensate for the CoG of the TWR, the pitch angle was modified by successively stopping at a subgoal placed on the travel path. Gopinath et al. proposed a variable LQR gain to achieve TWR stabilization when carrying a heavy payload [8]. In this approach, the effect of the payload is considered as a change in the mass and length of the vehicle body.

The methods in [6]- [8] are designed to cope with CoG fluctuations when a load is placed on the top of the TWR, but the mechanical characteristics of the TWR prevent it from acting on removing a load from a shelf. For the TWR to perform the same actions as a person, it is necessary to use an arm. The two-wheeled robot with an arm (TWRwA) has the characteristic of a large CoG shift in the front-back direction depending on the load. As a robot whose CoG can shift back and forth significantly, some studies have considered controlling the CoG position in two-wheeled mobile robot manipulators [9] [10]. However, these studies did not consider placing a load on the robot. Therefore, it is necessary to introduce a controller that can compensate for the change in CoG caused by the load when the TWRwA is used to carry a load. In [7], it is necessary to stand still each time to correct the CoG, which is not efficient. In addition, [8] does not address the CoG shift in the front-back direction of the vehicle body.

Yajima et al. applied RCC to TWRwA to deal with fluctuations in the CoG when a load is placed on the arm [11]. However, this approach has the disadvantage that the design is complicated because there are many controller parameters to be set and the parameters must be determined experimentally. In addition, the RCC determines the command value compliantly to accommodate the motion of the person boarding, but there is a problem with slow convergence to a desired pitch angle that can compensate for the CoG for a stationary load. A slow convergence to the inner pitch angle also deteriorates the performance of the outer wheel position control, which can lead to the risk of hitting the shelf when placing loads on the arm.

To solve this problem, this paper proposes a model-based method to determine the pitch angle and position control so that the CoG, including the load, can be placed right above the axle. The proposed method uses a reaction torque observer (RTOB) [12] introduced into the arm motor to estimate the load-derived torque applied to the arm. The moment applied to the axle is then calculated from the estimated torque and the model of the vehicle body, and the pitch angle command value required to compensate for the CoG is calculated. The pitch angle is controlled by PD control with SPADO to track the command value, and wheel position control is realized by PI control on the outer side of the pitch angle. In the proposed method, the controller parameters are simply set and the pitch angle quickly converges because the command values are statically determined on a model basis. As a result, experiments have confirmed that fast convergence of wheel position control can be achieved.

This paper is organized as follows: In section II, the modeling of the TWRwA is described. In Section III, the control system of the TWRwA is explained. In section IV, the validity of the proposed method is evaluated through experiments. Finally, section V describes the conclusion.

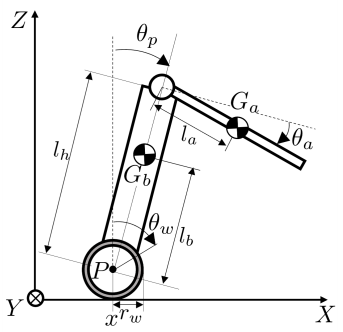

Fig. 1. Side view of two-wheeled robot with an arm.

TABLE I
VARIABLES ABOUT TWO-WHEELED ROBOT WITH AN ARM

Variable	Explanation
P	Control reference point of system
G_b	CoG position of body
G_a	CoG position of arm
r_w	Radius of wheels
l_b	Distance between P and G_b
l_h	Height of body
l_a	Distance between arm motor and G_a
θ_p	Pitch angle of the body
θ_w	Rotation angle of wheels
θ_a	Pitch angle of arm
x	Position of P (wheel position)
m_w	Mass of wheels
m_b	Mass of body
m_a	Mass of arm
I_{wy}	Inertia of wheels around y-axis
I_{by}	Inertia of body around y-axis
I_{ay}	Inertia of arm around y-axis
n_w	Gear ratio of wheel motor torque
n_a	Gear ratio of arm motor torque
τ_w	Wheel motor torque
τ_a	Arm motor torque

II. MODELING

This section describes the modeling of the TWRwA. In this paper, turning movements are not considered to investigate the effect on wheel position control when a load is placed on the TWRwA. The model of the TWRwA can be expressed in XZ-plane as shown in Fig. 1. Variables in this paper are shown in Table I.

The relationship between x and θ_w is represented by (1) with no slip assumed.

$$\dot{x} = r_w \dot{\theta}_w \tag{1}$$

The equation of motion of the TWRwA is derived as (2) by using the Lagrangian method.

$$\boldsymbol{M}(\boldsymbol{x})\ddot{\boldsymbol{x}} + \boldsymbol{H}(\boldsymbol{x}, \dot{\boldsymbol{x}}) + \boldsymbol{G}(\boldsymbol{x}) \quad = \quad \boldsymbol{E}\boldsymbol{\tau} \tag{2}$$

$\boldsymbol{M}$ is the inertia matrix, $\boldsymbol{H}$ is the centrifugal and Coriolis term, $\boldsymbol{G}$ is the gravity term, and $\boldsymbol{E}\boldsymbol{\tau}$ is the generalized force. The structure of each matrix is shown from (3) to (22).

$$\boldsymbol{M} = \begin{bmatrix} m_{11} & m_{12} & m_{13} \\ m_{21} & m_{22} & m_{23} \\ m_{31} & m_{32} & m_{33} \end{bmatrix} \tag{3}$$

$$\boldsymbol{H} = \begin{bmatrix} h_1 & h_2 & h_3 \end{bmatrix}^\top \tag{4}$$

$$\boldsymbol{G} = \begin{bmatrix} 0 & g_2 & g_3 \end{bmatrix}^\top \tag{5}$$

$$\boldsymbol{E} = \begin{bmatrix} \dfrac{n_w}{r_w} & 0 \\ -n_w & 0 \\ 0 & n_a \end{bmatrix}^\top \tag{6}$$

$$\boldsymbol{\tau} = \begin{bmatrix} \tau_w & \tau_a \end{bmatrix} \tag{7}$$

$$\boldsymbol{x} = \begin{bmatrix} x & \theta_p & \theta_a \end{bmatrix}^\top \tag{8}$$

$$m_{11} = m_b + 2m_w + \frac{2I_{wy}}{r_w^2} \tag{9}$$

$$m_{12} = \{(m_b + 2m_w)l_b + m_a l_h\}\cos\theta_p - m_a l_a \sin(\theta_p + \theta_a) \tag{10}$$

$$m_{13} = -m_a l_a \sin(\theta_p + \theta_a) \tag{11}$$

$$m_{21} = m_{12} \tag{12}$$

$$m_{22} = (m_b + 2m_w)l_b^2 + m_a(l_h^2 + l_a^2 - 2l_h l_a \sin\theta_a) + I_{by} \tag{13}$$

$$m_{23} = m_a l_a^2 - m_a l_h l_a \sin\theta_p + I_{ay} \tag{14}$$

$$m_{31} = m_{13} \tag{15}$$

$$m_{32} = m_{23} \tag{16}$$

$$m_{33} = m_a l_a^2 + I_{ay} \tag{17}$$

$$h_1 = -m_a l_a \cos\theta_p + \theta_a \left(\dot{\theta}_p + \dot{\theta}_a\right)^2 - \{(m_b + 2m_w)l_b + m_a l_a\}\sin\theta_p \dot{\theta}_p^2 \tag{18}$$

$$h_2 = -m_a l_h l_a \cos\theta_a \left(\dot{\theta}_a^2 + 2\dot{\theta}_a\dot{\theta}_p\right) \tag{19}$$

$$h_3 = -m_a l_h l_a \cos\theta_a \dot{\theta}_p^2 \tag{20}$$

$$g_2 = -(m_b l_b + m_a l_h) g \sin\theta_p - m_a l_a g \cos(\theta_p + \theta_a) \tag{21}$$

$$g_3 = -m_a l_a g \cos(\theta_p + \theta_a) \tag{22}$$

III. Control System

Section Ⅲ explains a control system. The block diagram of the whole system is shown in Fig. 2. Although the body system and the arm system interfere with each other, the body system and the arm system can be controlled independently by building observers in each system. The control system for each part is shown below.

A. Arm Position Control

Position control of the arm uses a PD controller with a DOB to improve robustness against disturbances. The part of the equation of motion expressed in (2) that relates to the arm is extracted and transformed into (23).

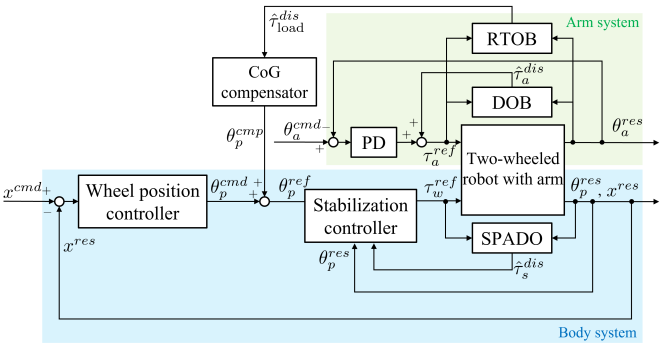

Fig. 2. Block diagram of the whole system.

$$m_{n33}\ddot{\theta}_a + \tilde{\tau}_a^{dis} = n_a \tau_a^{ref} \tag{23}$$

The subscript n is the nominal value of each matrix component in (3). The $\tilde{\tau}_a^{dis}$ in (23) is all disturbances including modeling errors, interference terms, centrifugal and Coriolis terms, gravity terms, and the effects of load. The estimated disturbance $\hat{\tau}_a^{dis}$ is obtained by (24).

$$\hat{\tau}_a^{dis} = \frac{\omega_a}{s + \omega_a}\left(n_a \tau_a^{ref} - m_{n33}\omega_a \dot{\theta}_a^{res}\right) - m_{n33}\omega_a \dot{\theta}_a^{res} \tag{24}$$

ω_a is the cutoff frequency of the low-pass filter (LPF). The disturbance $\hat{\tau}_a^{dis}$ estimated in (24) is fed back and compensated, and the arm position control is realized by PD control and a compensation term by DOB as shown in (25).

$$\tau_a^{ref} = K_{ap}(\theta_a^{cmd} - \theta_a^{res}) + K_{ad}(\dot{\theta}_a^{cmd} - \dot{\theta}_a^{res}) + \hat{\tau}_a^{dis} \tag{25}$$

K_{ap} and K_{ad} are the P-gain and D-gain of arm PD control respectively.

B. Posture Stabilization Control

Although TWRwA is a nonlinear system, it can be controlled as a linear system in the outer loop by making a linear approximation at the equilibrium point and compensating the approximation errors with a disturbance observer. Synthesized pitch angle disturbance observer (SPADO) is used to estimate disturbances applied to the body and disturbances applied to the wheels together.

The motion equation of wheel position direction and pitch angle direction are given as (26) and (27).

$$m_{n11}\ddot{x}^{res} = \frac{n_w}{r_w}\tau_w^{ref} - \tilde{\tau}_x^{dis} \tag{26}$$

$$m_{n21}\ddot{x}^{res} + m_{n22}\ddot{\theta}_p^{res} = -n_w \tau_w^{ref} - \tilde{\tau}_p^{dis} \tag{27}$$

$\tilde{\tau}_x^{dis}$ and $\tilde{\tau}_p^{dis}$ are disturbances in the wheel position direction and the pitch angle direction respectively as shown in (28) and

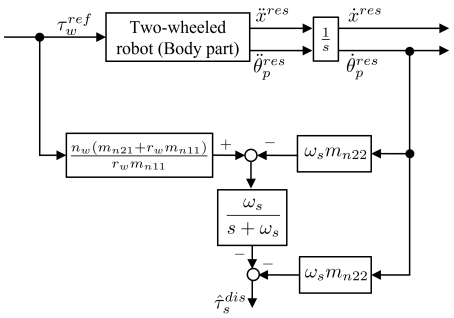

Fig. 3. Block diagram of SPADO.

(29), which include the disturbance $\tau_x^{dis}/\tau_p^{dis}$, modeling errors, interference terms, centrifugal and Coriolis term, gravity term, and the effects of load.

$$\begin{aligned}\tilde{\tau}_x^{dis} &= m_{12}\ddot{\theta}_p^{res} + (m_{11}-m_{n11})\ddot{x}^{res} + h_1 + \tau_x^{dis} \quad (28)\\ \tilde{\tau}_p^{dis} &= (m_{21}-m_{n21})\ddot{x}^{res} + (m_{22}-m_{n22})\ddot{\theta}_p^{res} \\ &\quad + h_2 + g_2 + \tau_p^{dis} \quad (29)\end{aligned}$$

We obtain (30) by eliminating $\ddot{x}^{res}$ from (26) and (27). $\tilde{\tau}_s^{dis}$ is called synthesized pitch angle disturbance and is expressed in (31).

$$m_{n22}\ddot{\theta}_p^{res} + \frac{m_{n21}+r_w m_{n11}}{r_w m_{n11}} \cdot n_w \tau_w^{ref} = -\tilde{\tau}_s^{dis} \quad (30)$$

$$\tilde{\tau}_s^{dis} = \tilde{\tau}_p^{dis} - \frac{m_{n21}}{m_{n11}}\tilde{\tau}_x^{dis} \quad (31)$$

Synthesized pitch angle disturbance $\tilde{\tau}_s^{dis}$ is estimated as (32) by using the LPF.

$$\begin{aligned}\hat{\tau}_s^{dis} = &-\frac{\omega_s}{s+\omega_s}\left(\frac{m_{n21}+r_w m_{n11}}{r_w m_{n11}} \cdot n_w \tau_w^{ref} - m_{n22}\omega_s \dot{\theta}_p^{res}\right) \\ &- m_{n22}\omega_s \dot{\theta}_p^{res} \quad (32)\end{aligned}$$

ω_s is the cutoff frequency of LPF. A block diagram of SPADO is shown in Fig. 3. By feeding back the estimated disturbance $\hat{\tau}_s^{dis}$, the pitch angle becomes robust to the disturbance, and a linearized control system can be realized.

To stabilize the body system, torque reference is determined based on the Lyapunov stability theorem. Lyapunov function V is set as (33).

$$V = \frac{1}{2}K_1(\theta_p^{ref} - \theta_p^{res})^2 + \frac{1}{2}K_2(\dot{\theta}_p^{ref} - \dot{\theta}_p^{res})^2 \quad (33)$$

K_1 and K_2 are positive gains. We obtain (34) by differentiating (33).

$$\dot{V} = \left(\dot{\theta}_p^{ref} - \dot{\theta}_p^{res}\right)\left\{K_1\left(\theta_p^{ref} - \theta_p^{res}\right) + K_2\left(\ddot{\theta}_p^{ref} - \ddot{\theta}_p^{res}\right)\right\} \quad (34)$$

We obtain (35) by eliminating $\ddot{\theta}_p^{res}$ from (30) and (34).

$$\begin{aligned}\dot{V} = &\left(\dot{\theta}_p^{ref} - \dot{\theta}_p^{res}\right)\Big[K_1\left(\theta_p^{ref} - \theta_p^{res}\right) \\ &+ K_2\left\{\ddot{\theta}_p^{ref} + \frac{1}{m_{n22}}\left(\frac{n_w\left(m_{n21}+r_w m_{n11}\right)}{r_w m_{n11}}\tau_w^{ref} + \tilde{\tau}_s^{dis}\right)\right\}\Big] \quad (35)\end{aligned}$$

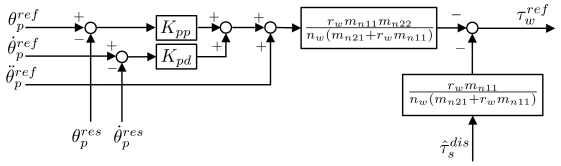

Fig. 4. Block diagram of posture stabilization control.

When (35) is less than or equal to 0 as shown in (36), the pitch angle can be stabilized.

$$\dot{V} = -K_3\left(\dot{\theta}_p^{ref} - \dot{\theta}_p^{res}\right)^2 \quad (36)$$

K_3 is a positive gain. Therefore, torque reference is determined as (37).

$$\begin{aligned}\tau_w^{ref} = &-\frac{r_w m_{n11} m_{n22}}{n_w\left(m_{n21}+r_w m_{n11}\right)}\left\{K_{pp}\left(\theta_p^{ref} - \theta_p^{res}\right)\right. \\ &\left. + K_{pd}\left(\dot{\theta}_p^{ref} - \dot{\theta}_p^{res}\right) + \ddot{\theta}_p^{ref}\right\} - \frac{r_w m_{n11}}{n_w(m_{n21}+r_w m_{n11})}\hat{\tau}_s^{dis} \quad (37)\end{aligned}$$

The torque input determined by (37) satisfies Lyapunov's stability theorem and converges the pitch angle to the command value [3]. K_{pp} and K_{pd} are defined as (38) and (39).

$$K_{pp} = \frac{K_1}{K_2} \quad (38)$$

$$K_{pd} = \frac{K_3}{K_2} \quad (39)$$

A block diagram of posture stabilization control is shown in Fig. 4.

C. Wheel position control

The TWRwA moves by tilting the body in the direction it wants to move. In this research, wheel position control is constructed outside of posture stabilization control. The wheel position control consists of a PI controller and a phase compensator. The phase compensator is used to remove unstable poles that cause pitch angle oscillations.

D. CoG compensation

A CoG compensator is designed to counteract the effect of CoG variation when a load is placed on the arm. RTOB is introduced to the arm motor as shown in (40) to estimate the torque due to the influence of the load.

$$\begin{aligned}\hat{\tau}_{\text{load}}^{dis} = &-\frac{\omega_l}{s+\omega_l}\left(n_a\tau_a^{ref} - g_3 - (F + D\dot{\theta}_a^{res}) - m_{33}\omega_l\dot{\theta}_a^{res}\right) \\ &- m_{33}\omega_l\dot{\theta}_a^{res} \quad (40)\end{aligned}$$

ω_l is the cutoff frequency of LPF. F, D, g_3, and m_{33} are coulomb friction, viscous friction, gravity term, and inertia of arm, which are identified values. Only the reaction torque from the load can be extracted by subtracting the friction, gravity term, and modeling error from the total disturbance.

The gravity acting on the vehicle when the TWRwA carries a load is shown in Fig. 5. l_l is the distance between the CoG

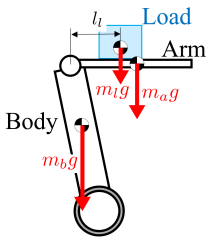

Fig. 5. Gravity acting on TWRwA.

of the load and the arm motor.

To keep the total CoG above the axle, the pitch angle must be set using (41).

$$m_b g l_b \sin\theta_p + m_a g\{(l_h \sin\theta_p + l_a \cos(\theta_p + \theta_a))\} + m_l g\{(l_h \sin\theta_p + l_l \cos(\theta_p + \theta_a))\} = 0 \quad (41)$$

Since the term caused by the load in (41) can be regarded as the estimated value of the arm RTOB shown in (40), (41) can be transformed into (42).

$$\hat{\tau}_{\text{load}}^{dis} + m_b g l_b \sin\theta_p + m_a g\{(l_h \sin\theta_p + l_a \cos(\theta_p + \theta_a))\} = 0 \quad (42)$$

When the arm is controlled to be parallel to the ground, $\theta_p + \theta_a$ in (42) can be regarded as 0. In addition, when the pitch angle is controlled close to 0, the approximation in (43) is valid.

$$\sin\theta_p \approx \theta_p \quad (43)$$

By transforming (42), the compensation value of the pitch angle θ_p^{cmp} is designed by (44).

$$\theta_p^{cmp} = -\frac{\omega_m}{s+\omega_m} \cdot \frac{m_a g l_a + \hat{\tau}_{\text{load}}^{dis}}{(m_b l_b + m_a l_h) g} \quad (44)$$

To avoid generating a large value due to sudden changes in estimated torque $\hat{\tau}_{\text{load}}^{dis}$, an LPF with a cutoff frequency of ω_m is applied to the calculated value.

IV. Experiment

In this section, the experiments are conducted. The control system shown in Fig. 2 was used to keep the position at 0. The behavior of the TWRwA was investigated when a 5 kg weight was placed on the arm so that l_l was 0.2 m. After the TWRwA stabilized, the load was placed on the arm at 5 s and removed at 40 s. The pitch angle command has an offset of 0.024 rad to take into account the gravity of the arm.

All parameters used in the experiments were shown in table II.

Fig. 6 shows the experimental result of pitch angle θ_p and wheel position x when only the position controller is used without the CoG compensator. The yellow background color in Fig. 6 indicates the time the load is on the arm. Fig. 6 shows that the pitch angle starts to tilt when the load was placed on the arm, and the position control worked to keep the position

TABLE II
Parameters used in experiments

Parameter	Explanation	Value conv.	Value prop.
K_{pp} $(1/s^2)$	P-gain of pitch angle control	200	200
K_{pd} $(1/s)$	D-gain of pitch angle control	28.3	28.3
K_{ap} $(1/s^2)$	P-gain of arm position control	100	100
K_{ad} $(1/s)$	D-gain of arm position control	20	20
K_{wp} (rad/m)	P-gain of wheel position control	4.50	4.50
K_{wi} (rad/ms)	I-gain of wheel position control	0.600	0.600
ω_s (rad/s)	Cutoff angular frequency of SPADO	$2\pi{\cdot}4$	$2\pi{\cdot}4$
ω_a (rad/s)	Cutoff angular frequency of arm DOB	$2\pi{\cdot}5$	$2\pi{\cdot}5$
ω_l (rad/s)	Cutoff angular frequency of RTOB	$2\pi{\cdot}15$	$2\pi{\cdot}15$
A_c $(-)$	Assist gain of RCC	1	-
K_c (Nm/rad)	Virtual spring of RCC	82.5	-
D_c (Nms/rad)	Virtual damper of RCC	32.6	-
M_c (kgm^2/rad)	Virtual mass of RCC	3.23	-
ω_m (rad/s)	Cutoff angular frequency of CoG compensator	-	$2\pi{\cdot}6$

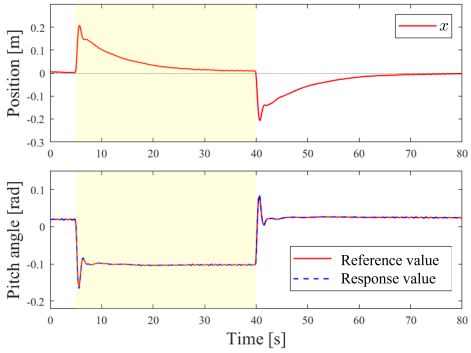

Fig. 6. Experimental result only using the position control.

at 0. Although the pitch angle began to tilt as the load was placed on the arm, it took approximately 30 seconds for the wheel position to converge to 0. The position response value converged to 0 as deviations accumulated and the I-term was activated. In this control system, it can be seen that the overall CoG is slow to respond to the forward shift caused by the load on the arm, which harms the positional control performance.

Fig. 7 shows the experimental result of pitch angle θ_p and position x using the conventional method. The compensation value of the pitch angle θ_p^{cmp} by RCC is expressed by (45), and each parameter was calculated experimentally. The yellow area indicates the time when the load was on the arm.

$$M_c \ddot{\theta}_p^{cmp} + D_c \dot{\theta}_p^{cmp} + K_c \theta_p^{cmp} = -A_c \hat{\tau}_{\text{load}}^{dis} \quad (45)$$

At the moment the load was placed on the arm, the wheel position moved forward approximately 0.2 m. Approximately 5 s later, it moved back to -0.03 m.

Fig. 8 shows the experimental result of pitch angle θ_p and position x using the proposed method. The parameter $(m_b l_b + m_a l_h) g$ was set to 98.4, which was calculated from the model. m_b and m_a were calculated using the masses measured beforehand, and l_b and l_h were calculated based on the data used in the design.

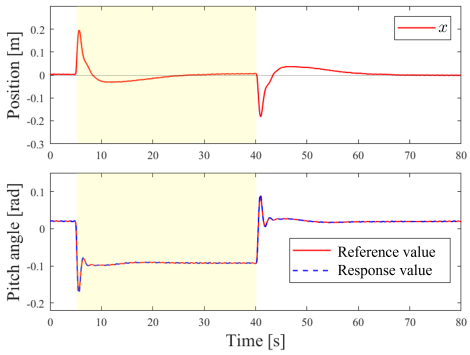

Fig. 7. Experimental result using the conventional method.

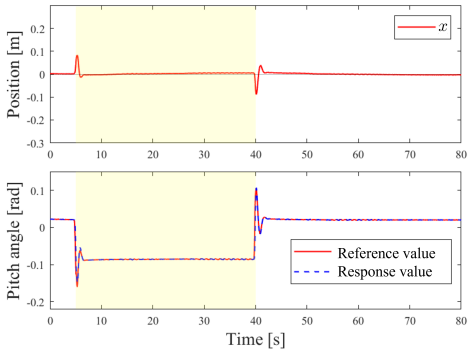

Fig. 8. Experimental result using the proposed method.

Fig. 8 shows that the pitch angle reference value is generated to keep the wheel position at 0 even when a load is placed on the arm and the pitch angle response value can be confirmed to track the reference value. The wheel position moved forward approximately 0.1 m at the moment the load was placed on the arm, and was able to track the command value of 0 in approximately 2 seconds.

A comparison of the experimental results of pitch angles for each method is shown in Fig. 9. The proposed method tracked the desired position the fastest among the three methods when the load is placed or removed. The conventional method using RCC tracked the wheel position to 0 more quickly than the only wheel position control method. On the other hand, the conventional method did not improve the amount of wheel position movement when a load was placed on or removed from the arm. The proposed method suppressed overshoot more than the conventional method, and the amount of wheel position movement when a load is placed on or removed from the arm is reduced to approximately half that of the conventional method.

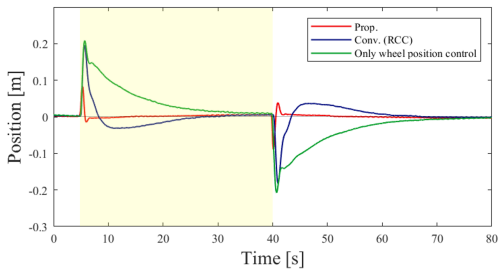

Fig. 9. Comparison of each method.

From the above, it is confirmed that the proposed method using model-based CoG compensation is effective.

V. Conclusion

The purpose of this study is to reduce the amount of wheel position movement when the load is on the arm. To achieve this objective, this paper proposed a model-based approach to statically determine the pitch angle to compensate for the CoG that varies with a load. Experiments have shown that it is possible to achieve a reduction in the movement of the robot when the load is applied.

References

[1] Ronald Ping Man Chan, Karl A. Stol, C. Roger Halkyard, "Review of modelling and control of two-wheeled robots," *Annual Reviews in Control*, vol. 37, Issue 1, pp. 89-103, 2013.

[2] K. Pathak, J. Franch and S. K. Agrawal, "Velocity and position control of a wheeled inverted pendulum by partial feedback linearization," *IEEE Transactions on Robotics*, vol. 21, no. 3, pp. 505-513, June 2005.

[3] A. Nakamura and T. Murakami, "A stabilization control of two wheels driven wheelchair," *2009 IEEE/RSJ International Conference on Intelligent Robots and Systems*, St. Louis, MO, USA, pp. 4863-4868, 2009.

[4] K. Hirata and T. Murakami, "A realization of step passage motion in two-wheel wheelchair systems utilizing variable repulsive compliance control," *2013 IEEE International Symposium on Industrial Electronics*, Taipei, Taiwan, pp. 1-6, 2013.

[5] M. Majczak and P. Wawrzyński, "Comparison of two efficient control strategies for two-wheeled balancing robot," *2015 20th International Conference on Methods and Models in Automation and Robotics (MMAR)*, Miedzyzdroje, Poland, pp. 744-749, 2015.

[6] C. Acar, T. Murakami, "Center of gravity compensation for dynamically balanced two-wheeled wheelchair system", *IEEJ Transactions on Industry Applications*, vol.131, no.5, pp.714-720, 2011.

[7] T. Takei, R. Imamura and S. Yuta, "Baggage Transportation and Navigation by a Wheeled Inverted Pendulum Mobile Robot," *IEEE Transactions on Industrial Electronics*, vol. 56, no. 10, pp. 3985-3994, Oct. 2009.

[8] A. Gopinath and V. R. Jisha, "Gain Scheduled LQR Control of a Two Wheeled Mobile Robot with Heavy Payloads," *2022 IEEE International Conference on Signal Processing, Informatics, Communication and Energy Systems (SPICES)*, THIRUVANANTHAPURAM, India, pp. 436-441, 2022.

[9] K. Sasaki and T. Murakami, "Pushing operation by two-wheel inverted mobile manipulator," *2008 10th IEEE International Workshop on Advanced Motion Control*, Trento, Italy, pp. 33-37, 2008.

[10] S. R. Larimi, P. Zarafshan and S. A. A. Moosavian, "Stabilized supervising control of a two Wheel Mobile Manipulator," *2013 First RSI/ISM International Conference on Robotics and Mechatronics (ICRoM)*, Tehran, Iran, pp. 265-270, 2013.

[11] H. Yajima, K. Ishizaki, Y. Miyata, M. Nawa, N. Kato and T. Murakami, "Posture Stabilization Control Compensating Variation of Body Center of Gravity in Underactuated System," *2023 IEEE International Conference on Mechatronics (ICM)*, Loughborough, United Kingdom, pp. 1-6, 2023.

[12] T.Murakami, R.Nakamura, F.Yu, and K.Ohnishi, "Force Sensorless Compliant Control Based on Reaction Force Estimation Observer in Multi-Degrees-of-Freedom Robot" *Journal of RSJ*, Vol. 11, No. 5, pp. 765-768, 1993.